Development of a micro PET system with improved spatial resolution through depth-of-interaction measurement

P. M. M. Correia[a], I. F. C. Castro[a], J. F. C. A. Veloso[a]

[a]I3N -Physics Department, University of Aveiro,
3810-193 Aveiro, Portugal

ABSTRACT

In small diameter positron emission tomography (PET) systems, the determination of the depth-of-interaction (DOI) of 511 keV gamma photons in scintillator crystals is of great importance, in order to achieve high DOI resolution with good uniformity within the entire field-of-view. In this work, we propose a new method for DOI determination, in which a single layer of LYSO crystals is read out on both ends through the use of silicon photomultipliers (SiPMs), but using wavelength-shifting fibers and a reduced number of SiPMs on one end. This design results in a simpler and less expensive readout when compared to the typical dual-ended readout method, which requires two photodetectors per crystal and corresponding readout electronics. GATE simulation of the system was carried out and experimental proof-of-concept studies were performed on a single detector cell (composed of two LYSO crystals operating in coincidence), to evaluate the amount of light detected on each side of the crystal and the achievable DOI resolution with this method, taking into account the attenuation of the light signal on the fiber side with crystal-SiPM distance. The feasibility of applying this new method in full detector rings for a small animal PET system is evaluated and discussed, considering different alternatives for position readout electronics.

Keywords: PET, DOI, SiPM, wavelength-shifting optical fibers, GATE

1. INTRODUCTION

The development of molecular imaging systems for small animals assumes vital importance in order to study and improve the medical systems used in clinical research. The Positron Emission Tomography (PET) is one of the most used and studied imaging systems. The high molecular selectivity, high spatial resolution and lower radiation doses for patients, when compared with other systems, makes PET one of the most interesting imaging techniques. Due to that fact, there is currently a large number of works trying improving and suggesting new small PET systems.

High spatial resolution is a required parameter when imaging of small animals is considered, since the physical dimensions of organs of such animals are usually of the order of the mm. Spatial resolution in cylindrical-type PET systems is affected by the parallax effect, specially when large scintillator crystals are used and the radiation sources are not located at the center of the system's field of view (FOV).

The need to obtain a similar signal-to-noise ratio in small animal imaging translates into the demand for spatial resolution improvement. Therefore, small PET systems with depth of interaction (DOI) capabilities assume vital importance for a large number of applications.

In PET systems, a line of response (LOR) is traced between two crystals that absorbed gamma rays at the same time. This LOR is usually traced considering the center of the inner surface of the scintillator that is facing the center of the cylinder, in a way that LORs of the same crystal are always the same, neglecting the interaction position. This translates into a parallax error when the gamma rays penetration direction is oblique to the crystals, and spatial resolution decreases with the increase of the distance to the center of the FOV. The knowledge of the DOI allows correcting the LOR, thus achieving a more uniform spatial resolution.

Further author information: (Send correspondence to P.M.M. Correia)
P.M.M. Correia: E-mail: pmcorreia@ua.pt

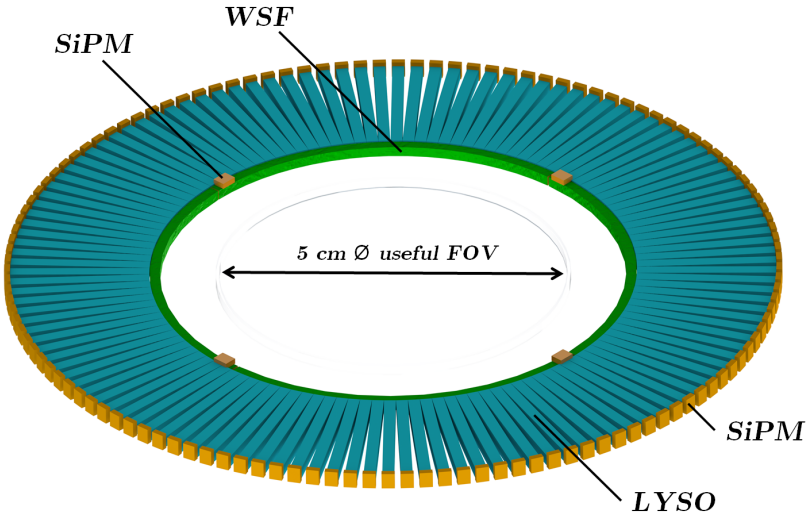

Figure 1: Sketch of the proposed microPET detector ring, using 128 LYSO crystals and 4 WSFs for DOI determination (all components drawn to scale).

There are some studies regarding the development of DOI-capable PET systems. Usually, two approaches are considered. The first one, present in some commercial PET imagers, uses two or more layers of pixelated crystals with different scintillation decay times, obtaining the DOI through pulse-shape discrimination. This method has been applied to small animal[1,2] and also to brain[3] imaging, improving spatial resolution uniformity within the FOV and reporting spatial resolution under 2 mm FWHM.

The other approach is related with single-layer crystals and consists of reading scintillation light from both ends of the crystals, obtaining DOI from the ratio of the two signals. Configurations of this kind usually use two solid state sensitive detectors to read the scintillation. For example, ClearPEM breast-dedicated scanner uses Avalanche Photodiodes (APDs) to read LYSO crystals, measuring DOI with 2 mm spatial resolution.[4]

1.1 Small PET with DOI capability

In this work we propose a small PET system, with 5 cm diameter of useful FOV, composed by 128 LYSO crystals, with dimensions of $1.5 \times 1.5 \times 20$ mm^3. A dual end readout with SiPMs is proposed, but the inner SiPM is replaced by a wavelength-shifting optical fiber (WSF). A fraction of the scintillation photons will be detected by the SiPM coupled to the end of the crystal, while another fraction will be absorbed by the WSF, being re-emitted by fluorescence, with lower energy. Part of this converted light will be guided by the fiber. The readout of the trapped light in the WSF is made by a single SiPM in one of its ends or, at most, by two SiPMs, one at each end. A single WSF will be coupled to several crystals. In this way, instead of using two SiPMs for each crystal, we may use only one SiPM per crystal, in the external end, and one WSF coupled to several crystals, in the inner end, whose readout is made with another SiPM (or two). The main advantage of this configuration is the simpler readout, since we reduce, nearly to half, the number of SiPMs to be read. The system is depicted in Figure 1. The SiPM detection section is 1×1 mm^2 and the WSFs are BCF-91A square double-clad fibers (Saint-Gobain Crystals), with a cross section of 1×1 mm^2. The lateral surfaces of the crystal were painted with a $BaSO_4$ reflective paint. In this way, most of the photons will be guided to one of the two crystal ends reducing lateral losses.

2. SIMULATION

A previous simulation of the PET system to be developed is important to analyze its capabilities and the physical response, to optimize dimensions and to choose the best materials to be used. GATE[5,6] is a Monte-Carlo software

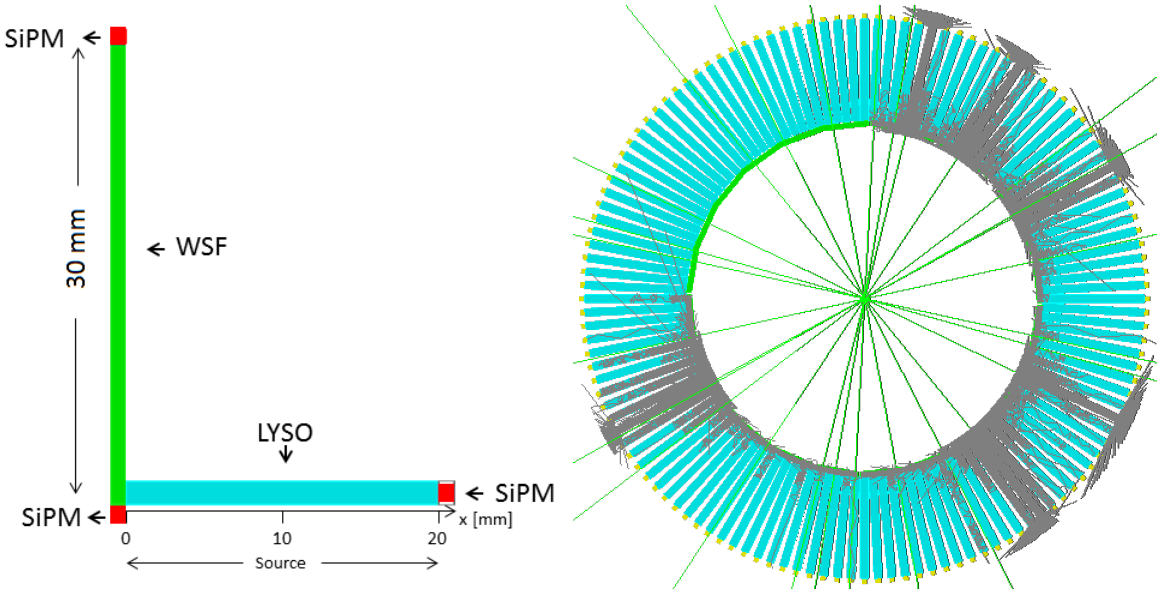

(a) (b)

Figure 2: a) Schematics of the simulated setup. A single LYSO crystal with a cross section of 1.5×1.5 mm^2 and 20 mm length is considered. For scintillation readout, one SiPM is coupled directly to one end of the crystal and a WSF is coupled to the other end. Each end of the WSF is then coupled to a SiPM (a readout with a single SiPM located at $y = 30$ mm was also simulated). b) GATE simulation image of the full cylindrical PET system, with a gamma ray point source located at the center of the ring. Green lines represent gamma photons, while grey lines are scintillation photons in the LYSO crystal.

that is massively used for simulations regarding medical imaging and radiotherapy systems. It is being developed by the OpenGATE collaboration, and is based on GEANT4[7] toolkit.

In the first simulations, a single crystal, coupled to a SiPM, and a single WSF, with another SiPM attached, were considered. We wanted to evaluate the number of photons detected by each SiPM, as a function of the interaction position inside the crystal. The long axis of the crystal is oriented with the x-axis of the global coordinates. The crystal is centered at $x = 10$ mm, having the WSF (with a length of 30 mm) coupled at $x = 0$ mm and the SiPM in the opposite position, at $x = 20$ mm.

The schematics of the simulated configuration is depicted in Figure 2a. In Figure 2b is represented a complete simulation of our prototype, with a gamma ray point source in the center of the FOV, that will be used for future simulations.

The following procedure was used for the simulation:

- 14308 primary photons with energy 2.9520 eV were simulated (corresponding to the maximum emission energy of the LYSO). This corresponds to the average number of scintillation photons produced per each gamma ray absorbed (511 keV of deposited energy), considering a LYSO scintillation light yield of 28 photons/keV.
- The position of the primary source is located at the coordinates $(x, 0, 0)$ mm inside the crystal. where x varies from 1 to 19 mm, corresponding to different gamma ray interaction positions inside the crystal.
- The number of detected photons in each SiPM is stored, for each distance x. A 30% SiPM photon detection efficiency is considered.

The depth of interaction along the crystal can be calculated by measuring the signals of the SiPMs coupled to the LYSO and to the WSF, *i.e.*, the number of photons detected in each side. The ratio R between the two

signals acts as a calibration function, which is described by equation 1.

$$R = \frac{A_1}{A_1 + kA_2} \tag{1}$$

where A_1 and A_2 are the signal measured in the LYSO SiPM and in the WSF SiPM(s), respectively, and k is a scale factor that translates the ratio between the LYSO and the WSF signal, for an emission at the center of the LYSO, being calculated by $k = A_1(x = 10\text{mm})/A_2(x = 10\text{mm})$.

2.1 Simulation results

The effect of depth of interaction in the amount of light detected in each side, considering different parameters, was simulated for:

- Two square WSFs of different cross section: 1×1 and 2×1 mm^2;
- WSF readout with one SiPM (at 30 mm from the crystal) or two SiPMs (one at each end);
- Specular, spread and diffuse reflection in the lateral surfaces of the LYSO. Four cases are considered, each corresponding to a different surface reflection in the crystal. The parameter σ covers a range between 0 and 6. When a photon reaches a surface, the simulation can use a perfect surface or a surface with small micro-facets. The normal surfaces of each facet are distributed around the average surface normal, with a standard deviation of σ, expressed in degrees. The higher the σ, the more spread is the reflection, while a smaller σ means a more specular reflection;
- Different reflectivity in the lateral surfaces of the LYSO, assuming a constant σ;

The results for each case are presented below.

2.2 1×1 WSF with a single SiPM readout, for different σ

For a square 1×1 mm^2 WSF, with a single SiPM located at the far end in relation to the LYSO, the amount of detected photons in each SiPM is represented in Fig. 3a.

When the source is near the WSF, *i.e.* $x \to 0$ mm, a maximum of light is read in the WSF-SiPM. On the contrary, when the source is near the other crystal end, $x \to 20$ mm, a maximum of light is collected by the SiPM that is directly reading the LYSO. The percentage of light detected in the LYSO-SiPM is considerable large, compared with the detected light in the WSF-SiPM. The losses in the interfaces between the LYSO and the WSF, and the photons that pass through the WSF without absorption and wavelength shifting re-emission, are the main reasons for this difference. It is also possible to see that more diffuse reflection in the LYSO surfaces results in more detected light in both SiPMs.

The plot of DOI ratio as a function of source position is represented in Fig. 3b. Different LYSO surfaces result in a slight variation of the ratio, namely a more diffuse reflection results in a higher curvature of the plot.

2.3 1×1 WSF with dual-end SiPM readout, for different σ

Regarding the previous simulation with a 1×1 WSF and a single SiPM for readout, we investigated the possibility of a dual-end SiPM in the WSF for readout. The results are shown in Fig. 4a. While the amount of detected light in the LYSO SiPM is the same, the introduction of a second SiPM for the WSF readout increases significantly the quantity of detected photons. The DOI function is shown in Fig. 4b. The main difference between the single or dual-end readout in the DOI is related with the size of the error bars, which are smaller in the dual-end situation. This will be discussed in more detail in section 2.6.

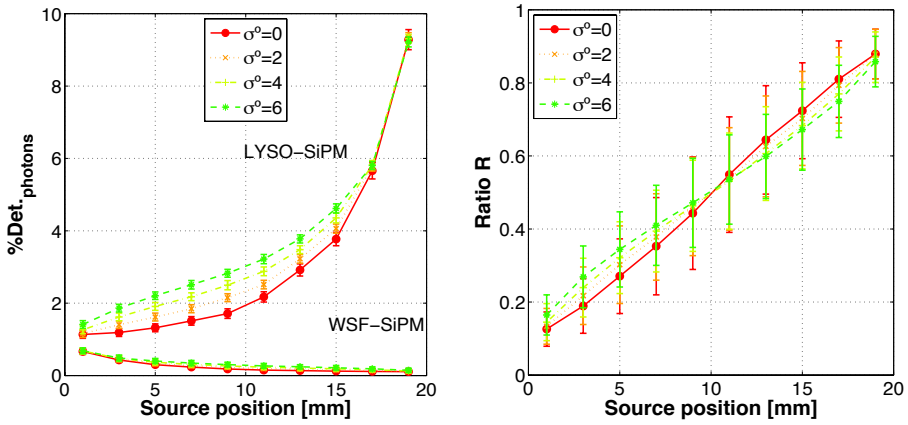

(a) (b)

Figure 3: a) Percentage of photons detected in LYSO and WSF SiPMs, for 1×1 mm^2 WSF with single SiPM readout, for different reflective lateral surfaces in LYSO and reflectivity of 97%. b) Corresponding DOI ratio.

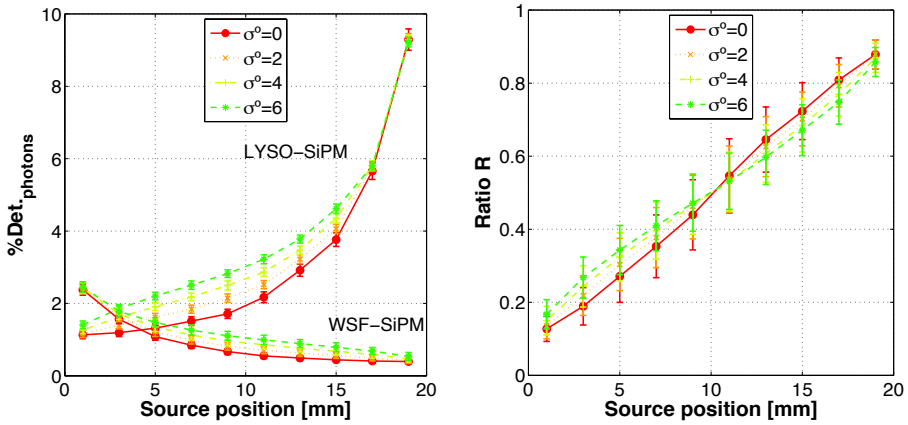

(a) (b)

Figure 4: a) Percentage of photons detected in LYSO and WSF SiPMs, for 1×1 mm^2 WSF with dual-end SiPM readout, for different diffusive lateral surfaces in LYSO and reflectivity of 97%. b) Corresponding DOI ratio.

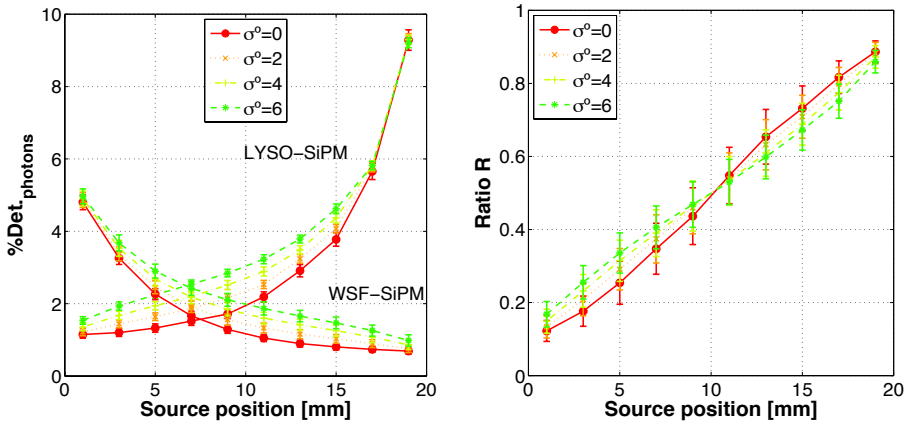

(a) (b)

Figure 5: a) Percentage of photons detected in LYSO and WSF SiPMs, for 2×1 mm^2 WSF with dual-end SiPM readout, for different diffusive lateral surfaces in LYSO and reflectivity of 97%. b) Corresponding DOI ratio.

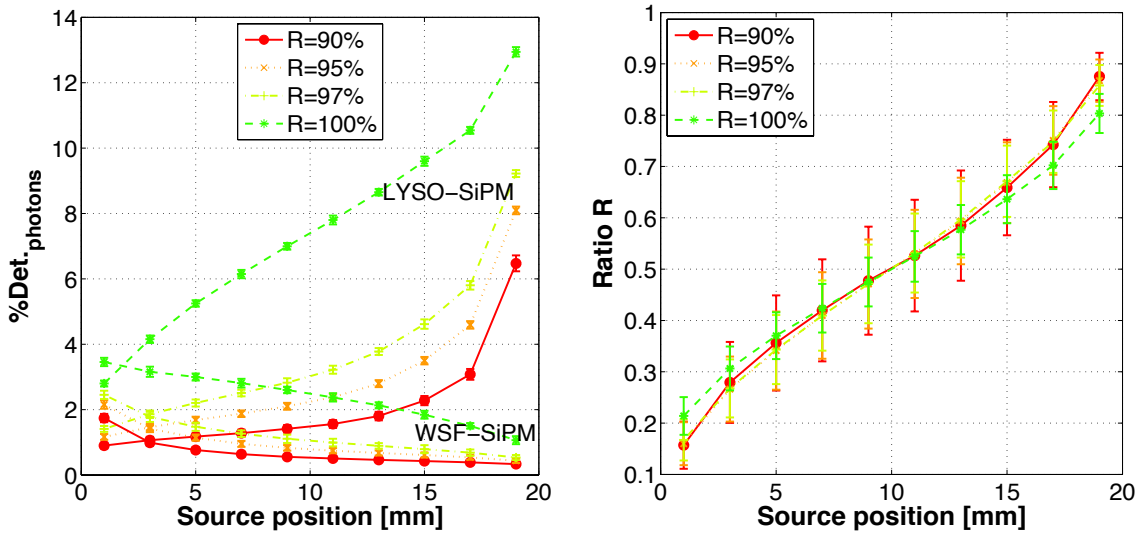

(a) (b)

Figure 6: Percentage of photons detected in LYSO and WSF SiPMs, for 1×1 mm^2 WSF with dual-end SiPM readout, for different reflectivity of LYSO surfaces, with diffuse reflection $\sigma = 6$. b) Corresponding DOI ratio.

2.4 2×1 WSF with dual-end SiPM readout, for different σ

Since the square section of the simulated LYSO is 1.5×1.5 mm^2, and the WSF previously simulated, and actually available from the manufacturer, is 1×1 mm^2, part of the light that reaches the LYSO end coupled to the WSF will not pass through it. A larger WSF, with 2×1 mm^2 section and a dual-end SiPM readout was simulated, ensuring that all the light that is lost in one end of the LYSO will pass through the WSF, increasing the number of wavelength shifts inside the WSF. The results are shown in Fig. 5a. In this configuration, an increase in the detected light from the WSF is observed, comparing with previous configurations. The DOI function, represented in Fig. 5b, is unchanged, but the error bars decrease when compared to 1×1 mm^2 WSF with single or dual-end readout.

2.5 1×1 WSF with dual-end SiPM readout, for different reflectivity

Since the angle of diffusion reflection of the lateral surfaces of the LYSO introduces considerable changes in the amount of detected light in both sides of the crystal, the influence of the surface reflectivity was also investigated. The LYSO that is being used was painted with a reflective paint of $BaSO_4$. A range of reflectivities between 90% and 100% was simulated, for a spread reflection with σ=6, using a 1×1 mm^2 WSF with dual-end readout. The results are shown in Fig. 6a. As would be expected, the increase in the reflectivity results in an increase in the percentage of detected light. The correspondent DOI ratio is represented in Fig. 6b. The main differences are observed at the ends of the LYSO (x→0 mm and x→20 mm). For 100% reflective surfaces, there is a less curved DOI function. The error bars also decrease with the increase of the reflectivity, due to the higher number of detected photons.

2.6 DOI resolution

For each of the previous situations, an analysis of the DOI resolution of the system was made. The results are shown in Figures . 7a, 7b and 7c. From the analysis of Fig. 7a, three important conclusions can be made. First, the DOI resolution strongly depends on the source position inside the LYSO: a better DOI resolution is achieved near the ends of the LYSO, worsening towards the center. Second, the DOI resolution achieved with a 2×1 mm^2 WSF is significantly better than with the 1×1 mm^2 WSF. Finally, the variation of the parameter σ also changes the DOI resolution. More diffuse reflection (higher σ) results in a flatter curve, while more specular reflection translates into higher differences between the maximum and minimum DOI resolution. From Fig. 7b, we can see that for the same WSF, with 1×1 mm^2, the introduction of a dual-end readout has a strong impact in the

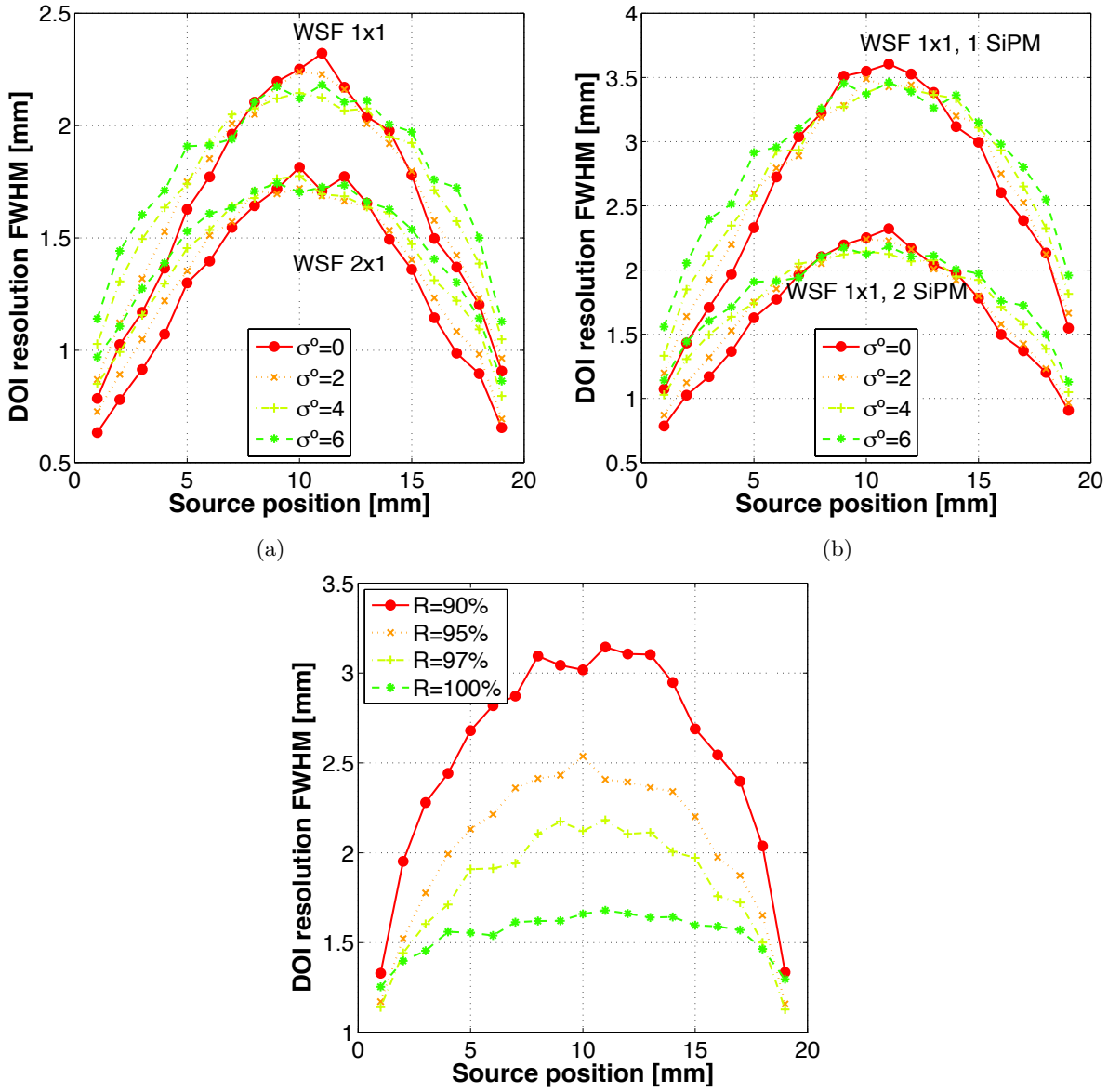

Figure 7: a) Influence of the WSF cross-section size in DOI resolution, for dual-end SiPM readout. b) Comparison of DOI resolution obtained with single and dual-end SiPM readout of a 1×1 mm^2 WSF. c) Comparison of DOI resolution obtained for different reflectivity of LYSO's lateral surfaces, using a 1×1 mm^2 WSF.

improvement of the resolution. Regarding the DOI resolution as a function of the reflectivity of the LYSO lateral surfaces, Fig. 7c shows that higher reflectivity considerably improves the DOI resolution, while less reflective surfaces result in poorer DOI resolutions. This clearly shows that the reflective paint of the LYSO is not only important to reduce the number of photon losses through the lateral surfaces, but it is also responsible for the achievement of a better DOI resolution, which is essential for our purpose.

3. EXPERIMENTAL MEASUREMENTS

Initial experimental measurements have been performed on a single LYSO crystal coupled to a WSF, in order to evaluate the amplitude of the light signal transmitted by the fiber in response to LYSO scintillation when

irradiated by 511 keV gamma photons, as well as the attenuation of this light signal for different fiber lengths. Two different photodetectors were used for these measurements.

In order to evaluate the feasibility of our DOI measurement method, a PET detector cell composed of two LYSO crystals operating in coincidence was assembled, using one of the crystals to define the real DOI by electronic collimation and applying our dual-ended readout to the other, thus obtaining a measured DOI.

3.1 LYSO-WSF-PMT attenuation

A first experimental system (Figure 8) was assembled to study the response of a single detector cell on the side of the LYSO crystal optically coupled to the WSF, which was subsequently read out by a PMT. A ^{22}Na source was placed on top of the other end of the crystal, using an aluminum plate in between, to block β^+ particles from interacting directly in the crystal. After preamplification and amplification, the PMT signal was fed to a multi-channel analyzer. The distance of the crystal to the PMT was varied from 11 to 61 mm.

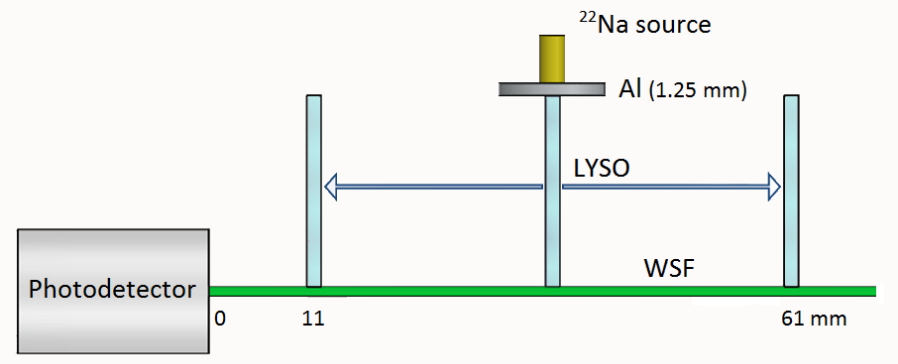

Figure 8: Sketch of the LYSO-WSF-photodetector attenuation measurement setup (side view).

The following material was used:

- ^{22}Na source of 0.1 inch active diameter (Spectrum Techniques, U.S.A.), with 10 μCi as of March 2013;
- LYSO crystal with dimensions 1.5×1.5×20 mm^3 (Kinheng Crystals, China);
- BCF91-A 1 mm round WSF, multi-cladded (Saint-Gobain Crystals, France);
- Hamamatsu R760 PMT (Hamamatsu, Japan);
- PMT readout electronics: Canberra 2005 preamplifier followed by Canberra 2022 NIM amplifier;
- Amptek 8000A MCA (multi-channel analyzer);
- A dark box ensuring operation without outside light;
- Optical grease (BC-630) was used between optical interfaces;

Experimental results obtained with the setup presented above are shown in Figures 9 and 10. Three acquisitions of 4 minutes were performed at each position. The smallest PMT-LYSO distance possible was 11 mm, a limitation due to the size of the plastic piece used to support the crystal and couple it to the WSF.

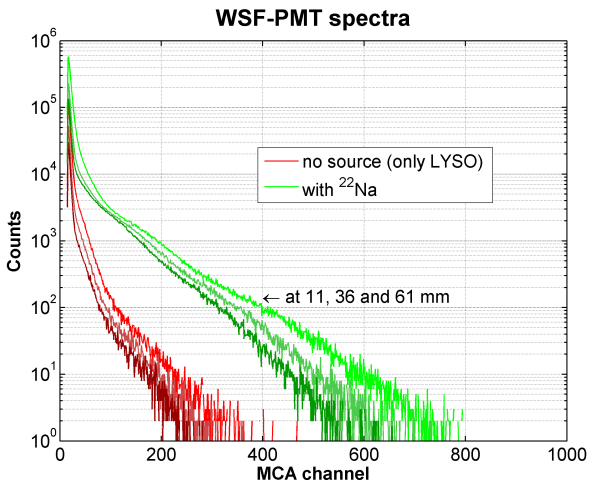

Figure 9: Example of spectra obtained for different LYSO-PMT distances, with and without ^{22}Na source.

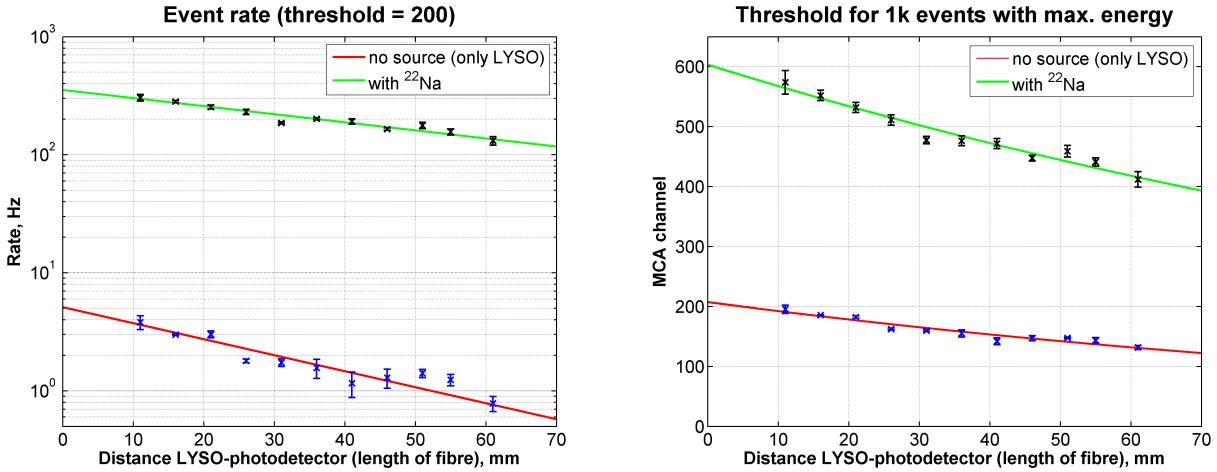

Figure 10: Attenuation of the light signal transmitted by the WSF with the LYSO-PMT distance: count rates above threshold 200 (left) and ADC channel above which the 1000 events with higher energy are recorded (right).

3.2 LYSO-WSF-SiPM attenuation

The PMT reading out the light in the WSF was replaced by a 1×1 mm^2 SiPM: S10362-11-100U MPPC (Hamamatsu, Japan). SiPM readout electronics were developed in-house, consisting of a charge preamplifier circuit (using OPA656) followed by an amplifier (AD8000). The first measurements were done similarly to the previous ones using a PMT. However, due to the dark noise of the SiPM and the gain/efficiency sensitivity of this device to small temperature changes, consistent measurements performed with only one SiPM reading out the fiber at different LYSO-SiPM distances, were more difficult to obtain. More reliable measurements can be obtained when two SiPMs are used: one to read out the crystal directly on one end and the other to read out the fiber. By operating the two SiPMs in coincidence, much of the dark noise will be eliminated, considering only the events of interest, i.e., the ones that result from the absorption of 511 keV γ-photons in the LYSO crystal.

Nevertheless, even without coincidence, the first results show a clearly higher signal from the SiPM in response to the ^{22}Na-LYSO light in the fiber, as compared to the intrinsic dark noise of the device (Figure 11). The signal from the LYSO crystal without any source was hardly discernible from the SiPM dark noise, except for very short LYSO-SiPM distances ($\lesssim$ 10 mm). Coincidence operation will also allow eliminating this LYSO intrinsic background signal, in the interaction crystals. The attenuation results are similar to those obtained with a PMT, showing a decrease of about 30-40% of the signal intensity in the 5-6 cm length of fiber.

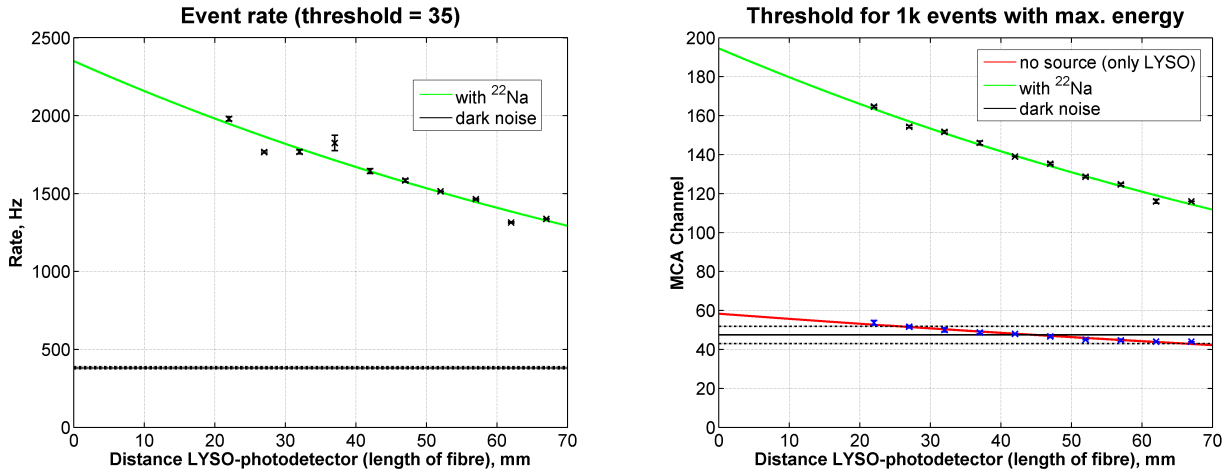

Figure 11: Attenuation of the light signal transmitted by the WSF with the LYSO-SiPM distance: count rates above threshold 35 (left) and ADC channel above which the 1000 events with higher energy are recorded (right).

3.3 DOI measurement setup

An experimental setup has been designed to test the DOI measuring capability of our method (Figure 12): two crystals placed in opposite positions to a central source were read out in coincidence, using one of them ($LYSO_1$) for source collimation and applying the dual-ended readout method to the other ($LYSO_2$), which was placed orthogonally to $LYSO_1$. In this way, the source can be aligned with different crystal depths and the capability of measuring the DOI from the ratio of crystal-SiPM/WSF-SiPM signals can be evaluated.

Due to the source-$LYSO_1$ distance used to ensure a reasonable collimation of the 511 keV gamma rays (about 6 cm), as well as to the small crystal thickness of $LYSO_2$ to absorb them (only 1.5 mm, since it was placed orthogonally), long acquisition times of some hours were necessary to obtain enough statistics. In addition, two ^{22}Na sources were used together to increase activity. As described in 3.1, these cylindrical sources have an active diameter of 0.1 inch, *i.e.*, 2.54 mm. A micrometer allowed the translational movement of a mechanical support holding a PMT coupled to $LYSO_1$ and the radioactive sources aligned with its center. The second crystal was placed in another support, used to facilitate the coupling of both its ends to the SiPM and WSF. Both mechanical supports were fixed to the same base, but only the part with PMT, LYSO and sources was allowed to move.

A SiPM with a relatively higher dynamic range (Hamamatsu S10362-11-50P) was used to read out $LYSO_2$ crystal end, while the model with higher gain and photon detection efficiency (S10362-11-100P) was used to read out the fiber end. The readout circuit was the same for both, except for the different gain of the second stage amplifier. LYSO-SiPM and WSF-SiPM were independently biased at +1.5 and +1 V overvoltage, respectively,

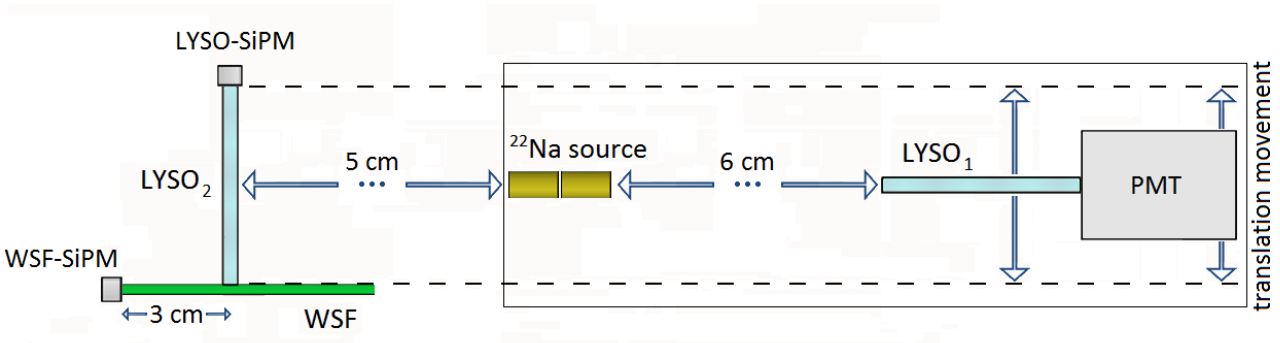

Figure 12: Sketch of the DOI measurement setup (top view). Only LYSO crystals, WSF and ^{22}Na source are drawn to scale relatively to each other.

automatically correcting temperature variations during acquisitions by a factor of 50 mV/°C. For this purpose, a power supply board (ISA Sensing, Portugal) with 8-bit resolution output between 69 and 73 V, controlled by a X3-10M board (Innovative Integration, U.S.A.) connected to a MAX31855 temperature sensor, was used. All measurements were performed at room temperature (25±2°C).

In order to evaluate the feasibility of our DOI determination method, the two SiPMs and the PMT signal were digitized in coincidence mode using a V1724 digitizer board (CAEN, Italy). An external gate signal was not necessary, since coincident triggers of the 3 channels within a given time window (150 ns) could be detected by this board, storing the energies and time stamps of the events in a file.

A square 1 mm BCF-91A fiber was used, which provides a better match to the photodetection area, in addition to its higher trapping efficiency relatively to the round one. The distance from the crystal to the fiber end coupled to the SiPM was kept fixed at 30 mm.

A (-15%,+25%) energy window around the 511 keV peak of $LYSO_2$-SiPM spectrum was defined and only coincidence events within this window were considered (Figure 13). Preliminary results of the SiPM signals for different depths of interaction along the crystal and corresponding DOI ratio are shown in Figure 14. The error

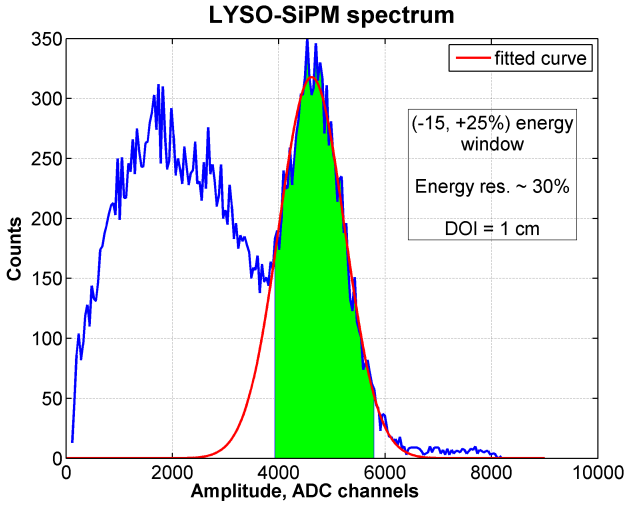

Figure 13: LYSO-SiPM spectrum obtained when ^{22}Na source was aligned with the center of $LYSO_2$ crystal (DOI = 1 cm), showing the energy window applied.

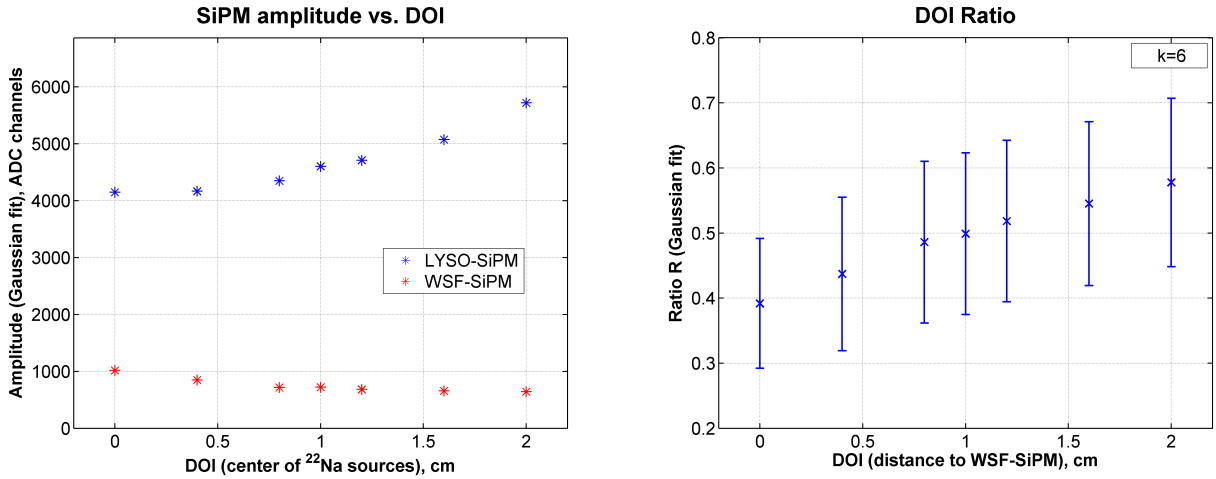

Figure 14: Preliminary DOI measurement results (WSF-SiPM positioned at 0 cm and LYSO-SiPM at 2 cm). Error bars represent the standard deviation of the Gaussian fit to the distribution of the DOI ratio R.

bars represent the standard deviation of the Gaussian fit to the distribution of R, which is related to the DOI resolution. However, this value hasn't been deconvoluted to take into account the dimension of the source and the enlargement of the beam of back-to-back 511 keV gamma photons electronically collimated by the PMT. These geometrical limitations of the experimental conditions have led to a real distribution of the gamma beam in $LYSO_2$ crystal with a width of about 5 mm around the center of the ^{22}Na source.

4. DISCUSSION AND CONCLUSIONS

In this work we propose the development of a small ring PET system with a new method for DOI determination, based on dual-ended readout of LYSO crystals with individual SiPMs on one side and WSFs coupled to SiPMs on the other. The optical response of a single detector cell to 511 keV gamma photons has been evaluated by means of simulations and experimental studies, measuring the amount of light at each side of the interacting LYSO crystal and demonstrating the feasibility of the DOI determination method.

From the simulations, the total percentage of detected photons in the LYSO and WSF SiPMs is less than 20% of the produced scintillation light, for the best case scenario, with a 2×1 mm^2 WSF and dual-end readout of 2×1 mm^2 SiPMs. This is related to several factors, such as the inefficient match between the cross section sizes of the SiPM and the crystal, the losses in the interfaces between media and also due to absorptions in the materials (without re-emissions, unlike the fluorescence process that occurs in the WSF), the trapping efficiency of the WSF, which depends on the geometry of the fiber, and the detection efficiency of the SiPM.

Regarding the DOI resolution calculated from simulations, it depends on the size of the WSF, the readout type in the WSF, the interaction position in the LYSO, the type of reflection in the LYSO lateral surfaces and the reflectivity of those surfaces. In accordance with the best scenario for total percentage of detected photons, the best DOI resolution was achieved with the 2×1 mm^2 WSF with dual-end readout.

In terms of the interaction position, interactions located near the ends of the LYSO result in a better DOI resolution. The average DOI resolution worsens with the higher diffusive behaviour of the lateral surfaces of the LYSO, and the higher the reflectivity of those surfaces, the better DOI resolution is achieved, due to the larger number of photons that escape from the LYSO through the ends and not the lateral surfaces.

Finally, future work in the simulations will focus on the influence of the losses in the interfaces between SiPMs, LYSO and WSF, and in the full simulation of the cylindrical PET with 128 LYSO and 4 WSFs for DOI calculation.

Experimental measurements of the amount of light transmitted to one end of a WSF coupled to one end of a LYSO crystal, under irradiation of a ^{22}Na source, show a considerable attenuation. Using only one end of the WSF for light readout, this attenuation of the WSF-SiPM signal with the distance to the interacting crystal will impact the DOI measurement method, making it necessary to use a calibration and correction method. The alternative is to use the dual-end SiPM readout of the WSF, which ideally results in a constant sum of the two signals, for the same DOI in any LYSO coupled to the fiber. As seen from the simulation, this dual-end readout of the WSF has also the advantage of improving DOI resolution. The disadvantage of using two SiPMs per fiber is that at least 2 crystals of each ring segment are not coupled to a fiber, due to the space required for the WSF-SiPMs. Therefore, DOI capability will not be possible for these positions. In addition, it is expected that the sum of the two SiPM signals from each side of the WSF will also result in an addition of electronic noise. The advantages of dual-end WSF readout should, however, surpass the drawbacks, improving the performance of the DOI measurement and thus, the spatial resolution performance of the whole PET system. Nevertheless, even with single SiPM readout at the far end of the WSF, the principle of DOI measurement has been experimentally demonstrated with success.

The development of position readout electronics for a ring of 128 crystals will consider two alternatives: one using a resistive chain requiring only a few readout channels and the other using individual LYSO-SiPM readout. Using the proposed method for DOI determination, our major goal is the assembly of an optimized prototype, capable of state of the art spatial resolution and suitable for small animal imaging, such as mice and rats used in pre-clinical nuclear imaging research.

ACKNOWLEDGMENTS

This work was supported by QREN programme Mais Centro - Programa Operacional Regional do Centro, FEDER and COMPETE, through projects RECI/FIS-NAN/0183/2012 and Biomaterials for Regenerative Medicine (CENTRO-07-ST24-FEDER-002030).

I.F.C. Castro is grateful to the latter for funding his scholarship: BPD/UI89/4300/2013.

P.M. Correia would like to thank FCT for funding his scholarship: BD/52330/2013.

REFERENCES

[1] Wang, Y., Seidel, J., Tsui, B. M., Vaquero, J. J., and Pomper, M. G., "Performance evaluation of the ge healthcare explore vista dual-ring small-animal pet scanner," *Journal of Nuclear Medicine* **47**(11), 1891–1900 (2006).

[2] Bergeron, M. et al., "Performance evaluation of the labpet apd-based digital pet scanner," *Nuclear Science, IEEE Transactions on* **56**, 10–16 (Feb 2009).

[3] de Jong, H. W. A. M., van Velden, F. H. P., Kloet, R. W., Buijs, F. L., Boellaard, R., and Lammertsma, A. A., "Performance evaluation of the ecat hrrt: an lso-lyso double layer high resolution, high sensitivity scanner," *Physics in Medicine and Biology* **52**(5), 1505 (2007).

[4] Neves, J. A., "The clearpem breast imaging scanner," *Nuclear Instruments and Methods in Physics Research Section A: Accelerators, Spectrometers, Detectors and Associated Equipment* **628**(1), 444 – 447 (2011). {VCI} 2010 Proceedings of the 12th International Vienna Conference on Instrumentation.

[5] Jan, S. et al., "Gate: a simulation toolkit for pet and spect," *Physics in Medicine and Biology* **49**(19), 4543 (2004).

[6] Jan, S. et al., "Gate v6: a major enhancement of the gate simulation platform enabling modelling of ct and radiotherapy," *Physics in Medicine and Biology* **56**(4), 881 (2011).

[7] Agostinelli, S. et al., "Geant4 - a simulation toolkit," *Nuclear Instruments and Methods in Physics Research Section A: Accelerators, Spectrometers, Detectors and Associated Equipment* **506**(3), 250 – 303 (2003).